crystals

MDPI

Article

Combining UV-Vis and Resonance Raman Spectroscopy to Characterize Molecular Aggregation

Valentina Sesti [1,2], Micol D'Antonio [1], Andrea Lucotti [1], Paola Moretti [1,2], Rossella Castagna [1], Chiara Bertarelli [1,2] and Matteo Tommasini [1,*]

[1] Dipartimento di Chimica, Materiali e Ingegneria Chimica "Giulio Natta", Politecnico di Milano, Piazza Leonardo da Vinci 32, 20133 Milano, Italy; valentina.sesti@polimi.it (V.S.); andrea.lucotti@polimi.it (A.L.); paola.moretti@polimi.it (P.M.); rossella.castagna@polimi.it (R.C.); chiara.bertarelli@polimi.it (C.B.)

[2] Center for Nano Science and Technology, Istituto Italiano di Tecnologia, Via Rubattino 81, 20134 Milano, Italy

* Correspondence: matteo.tommasini@polimi.it

Abstract: In this work, we use UV-Vis and Raman spectroscopy to correlate the intensity of selected transitions to the onset of aggregation phenomena. Through TDDFT calculations, we rationalize the formation of H-aggregates and their influence on the observed changes in the UV-Vis spectra. A correlation between Raman intensity and the molar absorption coefficient is experimentally observed and theoretically rationalized. We develop this method by considering Disperse Orange 3 (DO3), a well-known push–pull azobenzene dye with strong optical absorption in the blue–green region of the visible spectrum, and the known tendency to form H-aggregates.

Keywords: azobenzenes; molecular aggregation; Raman spectroscopy; UV-Vis spectroscopy; TDDFT; H-aggregates

check for updates

Citation: Sesti, V.; D'Antonio, M.; Lucotti, A.; Moretti, P.; Castagna, R.; Bertarelli, C.; Tommasini, M. Combining UV-Vis and Resonance Raman Spectroscopy to Characterize Molecular Aggregation. *Crystals* **2023**, *13*, 1141. https://doi.org/10.3390/cryst13071141

Academic Editor: Juan Ángel Sans

Received: 30 June 2023
Revised: 18 July 2023
Accepted: 19 July 2023
Published: 22 July 2023

Copyright: © 2023 by the authors. Licensee MDPI, Basel, Switzerland. This article is an open access article distributed under the terms and conditions of the Creative Commons Attribution (CC BY) license (https://creativecommons.org/licenses/by/4.0/).

1. Introduction

The aggregation phenomena of small organic molecules and functional polymers [1] are relevant in many applications, and they affect the formation of crystalline phases from concentrated solutions [2–4]. In pharmacology, aggregation phenomena in solution states are relevant as they influence drug behavior [5,6]. Self-assembly processes take place in solutions where molecules interact forming new supramolecular structures. For instance, it has been demonstrated that there is a direct dependence between the nucleation and growth of self-assembled monolayers and the concentration of the process solution [7]. Owing to their tendency to form H- or J-aggregates, which strongly influence their photophysical and nonlinear optical properties, conjugated small molecules have been the subject of extensive aggregation studies [8,9]. In H-aggregates, the chromophores are arranged in a parallel fashion with a side-by-side orientation of their transition moment, which results in a broadening and hypsochromic shift in the absorption spectra. In J-aggregates, the molecules are arranged in a slipped face-to-face geometry with a head-to-tail orientation of their transition moment, causing red-shifted absorption spectra.

The nature of the aggregate can vary depending on the overall molecular structure as well as on the electronic and steric features of the substituents [9]. In the field of synthetic dyes, the aggregation of azobenzenes has been investigated with both spectroscopical [10,11] and calorimetric techniques [12] in pure solution [11,13] and in the presence of template molecules and polymers in the media [10]. Both H-aggregate and J-aggregate have been observed for azodyes, depending on the molecule structure and on the testing conditions [10,14].

In this framework, we set out to develop a method that, by combining a computational and a spectral analysis approach, allows for the characterization and the rationalization of the occurring aggregation phenomenon at the molecular level.

UV-Vis absorption spectroscopy is certainly one of the most widely used methods that can probe the formation of aggregates in solutions [15]. In such applications, the advantage of this technique relates to its high sensitivity in a wide concentration range. However, UV-Vis absorption spectroscopy may not allow for deriving information about the kind of local interactions that are driven by aggregation phenomena. For this reason, in this work we propose to complement UV-Vis spectroscopy with resonance Raman (RR) spectroscopy which combines fair sensitivity with useful information about intermolecular interactions. Indeed, Raman has been used successfully to show the changing effects of intermolecular interactions in different conditions, spanning from the solid phase [16] to the formation of amyloid fibrils [17] to the solvated phase [18].

To establish a combined RR/UV-Vis spectroscopic method, we selected Disperse Orange 3 (DO3), a photochromic dye belonging to the class of push–pull azobenzenes [19]. The presence of a strong donor and an acceptor group in the 4,4′ positions, an amine (NH_2) and a nitro (NO_2), respectively, imparts a strong charge transfer character and a sizeable ground state dipole moment (9.9 D [20]). This results in strong dipole–dipole intermolecular interactions that can promptly drive aggregation, which is why DO3 was selected for this study. We chose dimethyl sulfoxide (DMSO) as the solvent because it is a well-known good solvent for DO3 and thus it allows the exploration of a wide range of concentrations. The combined RR/UV-Vis data were interpreted based on well-established theoretical models that highlighted the role of the transition dipole moment in both spectroscopic techniques. We accompany the experimental observations with TDDFT calculations that account for the effects of intermolecular interactions in H-aggregates containing an increasing number of DO3 units. The results show that the critical aggregation concentration that can be determined by UV-Vis spectroscopy corresponds to that derived from the observed changes in the resonance Raman intensities. Furthermore, the analysis of the concentration-dependent shift in resonance Raman spectra provides confirmation about intermolecular interactions.

Overall, as the main novelty of this work, we demonstrate an effective link between the well-established UV-Vis approach and a vibrational spectroscopic method. The good matching observed with the DO3 provides the foundations for a general analytical method that can be extended to any system with both a large enough molar absorptivity and a large resonance Raman cross-section.

2. Materials and Methods

Dimethyl sulfoxide (DMSO) and the Disperse Orange 3 dye (DO3) were used as purchased from Sigma-Aldrich. All solutions were obtained by dilution from a 10^{-1} M stock solution and were sonicated before dilution up to 10^{-6} M. The DMSO used was recently opened and stored under N2. A fresh stock solution was prepared before each sequence of experiments to avoid the setting up of aggregation phenomena with time.

UV-Vis experiments were recorded on a Cary5000 spectrophotometer. Quartz cuvettes with different optical path lengths were used, namely, 1 cm for concentrations ranging between [10^{-6} M–10^{-4} M], 5 mm for [2.5×10^{-4} M–10^{-3} M], and 0.5 mm for [2.5×10^{-3} M and 10^{-1} M]. This allowed us to obtain viable spectra, and to estimate the molar extinction coefficient $\varepsilon(\lambda_{max})$ at concentrations varying between 10^{-1} M to 10^{-6} M. In the following, $\varepsilon(\lambda_{max})$ will be simply denoted as ε. We evaluated the experimental error in the determination of ε by repeating the UV-Vis measurements at three different concentrations (10^{-4} M, 7.5×10^{-5} M, 5×10^{-5} M) on five different stock solutions prepared for this purpose. The relative error on ε (standard deviation/average) was 5%, independent of concentration. From basic error propagation theory, the relative error on the transition dipole ($\mu_{ge} \propto \varepsilon^{1/2}$) was $\sigma_\mu/\mu = ½\, \sigma_\varepsilon/\varepsilon = 2.5\%$.

The Raman spectra were measured using the dispersive Raman spectrometer Horiba Jobin Yvon LabRAM HR800UV, equipped with a 1800 grooves mm^{-1} grating, an Olympus BX41 microscope, and a Peltier-cooled CCD detector. A 405 nm laser, focused through a 50Xobjective, was used as the excitation source. The laser power was around 10 mW; the

exposure time was 30 s, and we averaged two exposures. These same conditions were kept for all the recorded spectra. The Raman cross-section of the DO3 solute (σ_a) was estimated based on the Raman cross-section of a reference band of the DMSO solvent (σ_s), since the Raman intensity of a given band of a given species in solution is given by $I = K\, I_0\, \sigma\, C$ [21], where I_0 is the laser intensity, C is the molar concentration, and K accounts for the efficiency of detection by the instrument. Therefore, by dividing the Raman intensity by the concentration of a given species, one obtains a quantity proportional to the cross-section, $I/C = K\, I_0\, \sigma$. This allows the cross-section ratio σ_a/σ_s to be expressed as follows:

$$\frac{\sigma_a}{\sigma_s} = \frac{I_a/C_a}{I_s/C_s} \tag{1}$$

Equation (1) correlates the Raman intensity of the analyte (I_a) and the solvent (I_s), the concentration of the sample (C_a), and the solvent concentration (C_S). C_S was evaluated as a constant considering the density of DMSO (1.1 g/cm^3) and the molecular weight of DMSO (78 g/mol). The ratio σ_a/σ_s was determined by using the intensity of the most intense band of DO3, corresponding to the NO symmetric stretching (1338 cm^{-1}) of the nitro group, normalized with respect to the intensity of the Raman signal of DMSO at 1050 cm^{-1}. The intensities of the two bands were determined on the spectra by subtracting the background using a baseline correction.

DFT calculations were carried out with Gaussian09 [22], using the B3LYP/6-311G(d,p) method, including dispersion effects (D3BJ—Grimme's D3 scheme including Becke–Johnson damping) and the implicit solvation scheme IEFPCM with the DMSO solvent. We computed the lowest 250 excited states of DO3 and its H-aggregates up to the hexamer with TD-B3LYP/6-311G(d,p) on fully geometry-optimized structures determined with the same DFT method. All calculations were carried out on a local cluster operated by our research group.

3. Results

UV-Vis spectra were recorded in a wide range of concentrations, namely between 10^{-1} M and 10^{-6} M. This was meant to observe the DO3 in DMSO at different stages of aggregation. In Figure 1 the UV-Vis spectra at different concentrations are shown, starting from the most diluted 10^{-6} M to the most concentrated at 10^{-1} M. The band corresponding to the most diluted solution is centered around 479 nm. When the concentration is increased (10^{-3} M) the shape of the spectrum is unchanged with respect to the diluted solution; however, the peak starts to shift at lower wavelengths. In fact, the band corresponding to the most concentrated solution is broader and is centered at a λ_{max} of about 473 nm. The shift to lower wavelengths at higher concentrations indicates the formation of H-aggregates [23]. In Figure 1b we report the molar extinction coefficient (ε) of DO3 for each solution. The coefficient ε was estimated through the Lambert–Beer law. As a result of this plot, we identified three regimes: the first regimes between 10^{-6} M and 10^{-4} M where the molecules are isolated, a second regime between 10^{-4} M and around 5×10^{-2} M where aggregation begins, and finally a third regime at highest concentrations where the molecules are in an aggregated state.

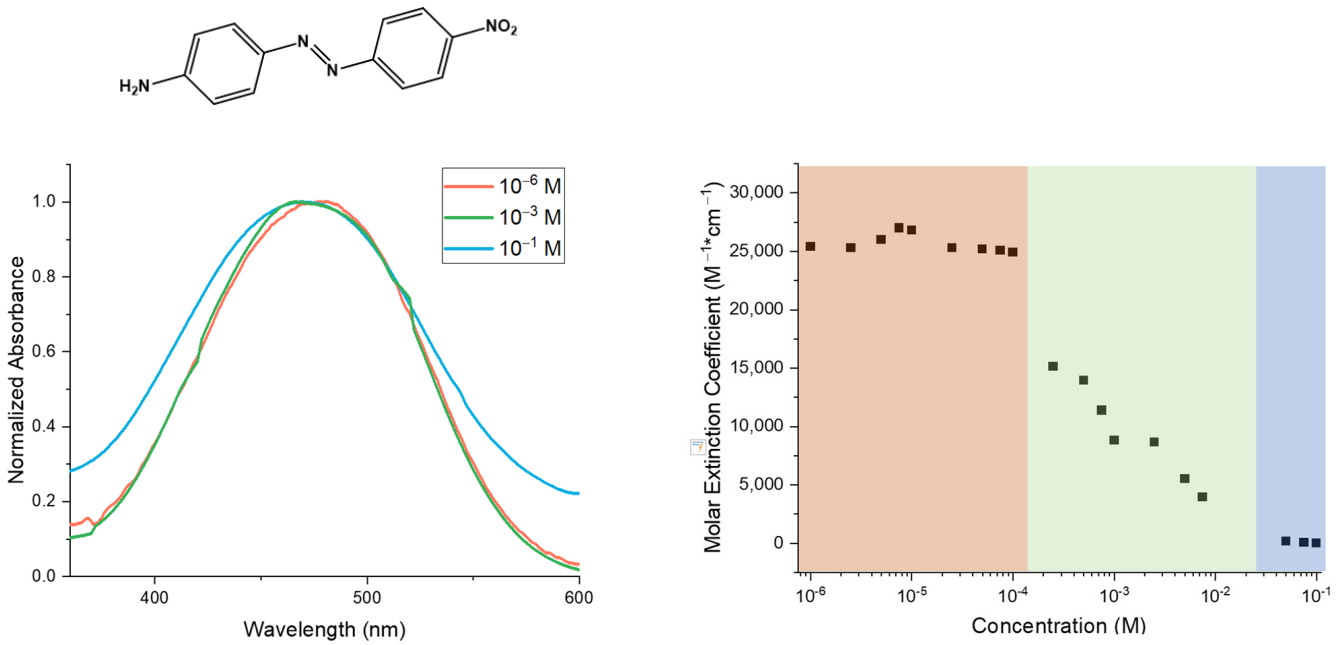

(**a**) (**b**)

Figure 1. (**a**) Plot of the UV-Vis absorption spectra of DO3 in DMSO at varying concentrations; on top of the plot we report the molecular structure of DO3. (**b**) Plot of the molar extinction coefficient (ε) of DO3 in DMSO at varying concentrations.

We report in Figure 2a the resonance Raman spectra of different solutions of DO3 in DMSO that were recorded with the same experimental conditions (see details in Materials and Methods). The ratio of the Raman cross-section of DO3 (σ_a) with respect to that of DMSO (σ_s) was determined using the intensity of one of the most intense bands of DO3, corresponding to the NO_2 symmetric stretch (1338 cm^{-1}), and the intensity of the Raman peak at 1048 cm^{-1} of the DMSO. These bands were chosen carefully, as the NO_2 band is one of the most intense of DO3, which allows us to estimate the intensity of this band at very low concentrations. The band chosen for the DMSO was the only one which was not in correspondence with other DO3 vibrational modes or hindered by the fluorescence signal. Accordingly, the spectra were recorded using a 405 nm laser, avoiding fluorescence but still in resonance for DO3 (see the UV-Vis absorption spectra in Figure 1a). In Figure 2b, the σ_a/σ_s ratio is plotted with respect to the concentration of the DO3 solutions in DMSO. The first observation is that the σ_a/σ_s ratio decreases as the concentration increases. Moreover, three regimes are also identified here and, remarkably, they are found at concentration ranges approximately matching those observed with the UV-Vis spectroscopy. Furthermore, the position of selected Raman transitions can be affected by aggregation. For instance, for decreasing concentration, the NO_2 band remains unshifted at 1338 cm^{-1}, whereas the N=N band shifts to higher wavenumbers from 1384 cm^{-1} to 1386 cm^{-1}, as reported in Figure 2c. Accordingly, this confirms that the azo (N=N) group is involved in the aggregation since the frequency of its stretching mode is affected by the concentration. This is consistent with the formation of H-aggregates with sandwich-like stacking.

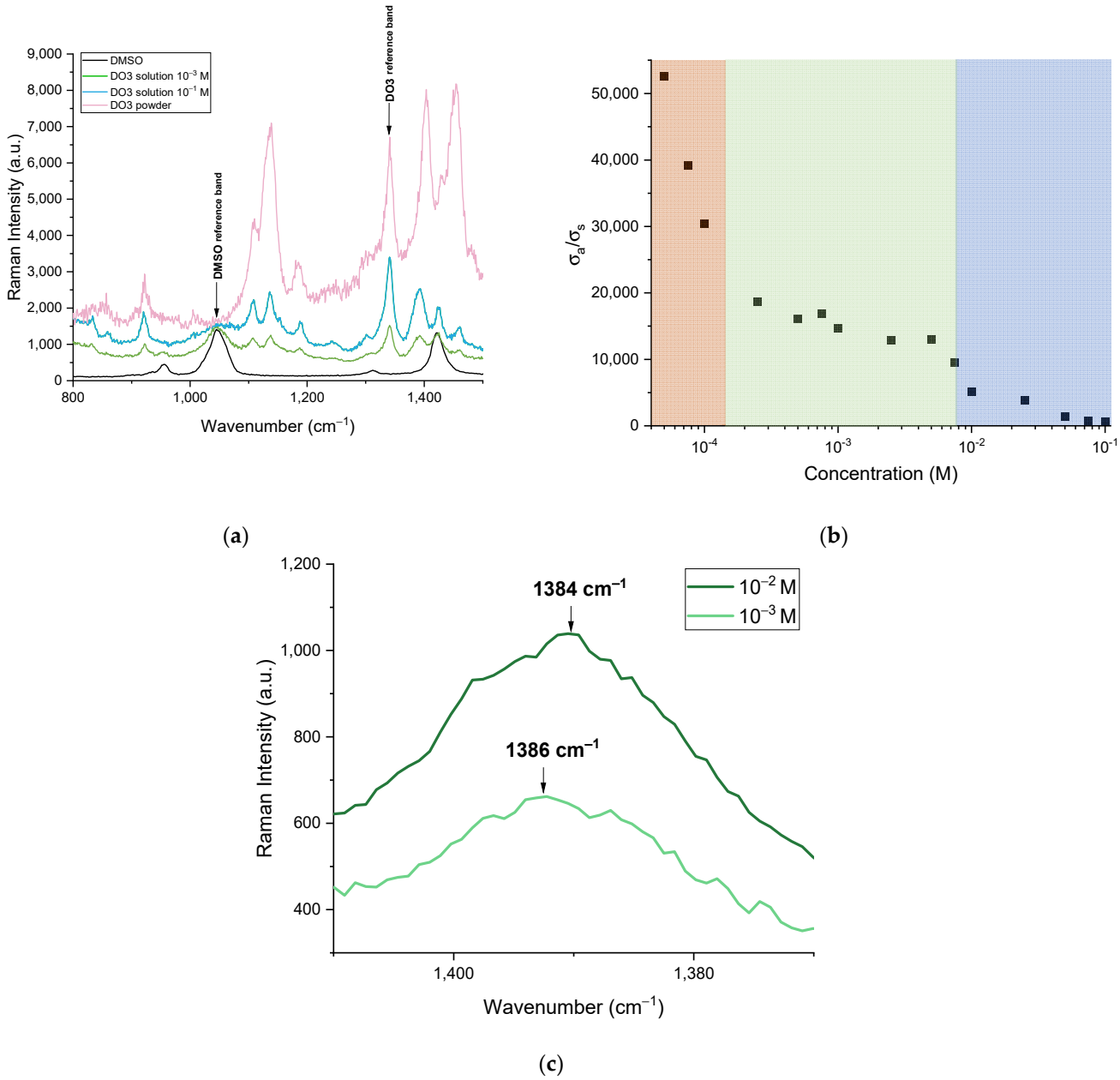

Figure 2. (**a**) Plot of the Raman spectra of DMSO, DO3 at the solid state, and DO3 in DMSO solution at varying concentrations. (**b**) The ratio of the Raman cross-section (σ_a/σ_s) at varying concentrations determined using the same reference Raman peaks for DO3 and DMSO. (**c**) The Raman spectra at two different concentrations centered around the N=N vibrational mode.

4. Discussion

The experimental data reported in Figures 1 and 2 suggest that the onset of the formation of H-aggregates occurs around a concentration of 10^{-4} M. TDDFT calculations were used to assess the effects of H-aggregation on UV-Vis absorption. We were interested in determining how the progressive stacking of DO3 molecules could affect the molar extinction coefficient so as to rationalize the experimental observation of its decrease for increasing concentration. We first checked if the selected DFT method could accurately represent the position and envelope of the observed experimental UV-Vis spectrum for a high concentration, where presumably the sample contains a significant amount of aggregates, which may be formed by a varying number of DO3 molecules. As reported in Figure 3, TDDFT calculations—as expected—confirm the progressive blueshift of the absorption

peak (assigned to the π→π* HOMO→LUMO transition) as the number of molecules per aggregate increases. Moreover, when the simulated spectra are normalized by the number of DO3 molecules forming the aggregate, the peak intensity significantly decreases, which qualitatively follows the experimental observation for the molar extinction coefficient. Remarkably, the presence of a broad UV-Vis band in the experimental spectrum can be attributed to the overlapping contributions of multiple components. These components originate from a distribution of H-aggregates made up of a varying number of molecules.

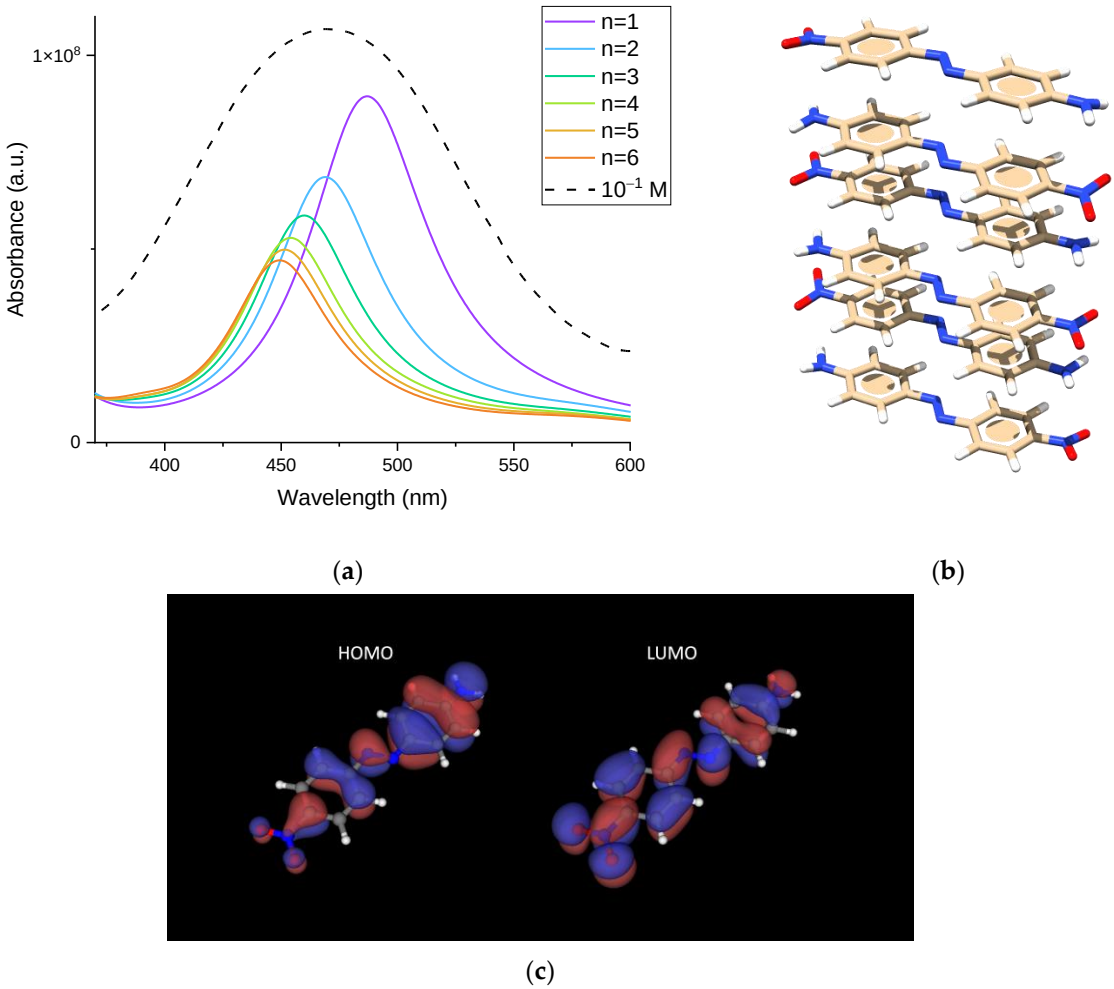

Figure 3. (**a**) Comparison between the experimental UV-Vis absorption spectrum of a concentrated solution of DO3 in DMSO (10^{-1} M, dotted black line) and the corresponding spectra simulated by TDDFT (colored lines) for the isolated molecule and H-aggregates of increasing size. (**b**) Three-dimensional representation of the optimized structure of the hexamer H-aggregate of DO3, as obtained by DFT calculations (see text). (**c**) Representation of the HOMO and LUMO orbitals of the DO3 monomer, as produced with the "surface" code of the BerkeleyGW suite of programs [24].

To better identify the mechanism responsible for the observed intensity decrease, we focused on the behavior of the transition dipole moment μ_{ge}, which is directly related to the molar absorptivity $\varepsilon \propto \mu_{ge}^2$ [25,26]. Hence, in Figure 4, we compare the relative decrease in the transition dipole moment computed by TDDFT for an increasing number of molecules in the H-aggregate with the relative decrease in the same quantity estimated from the experimental molar absorptivity by $\mu_{ge} \propto \sqrt{\varepsilon}$. To this aim, we compute from the TDDFT calculations the ratio $\left[\mu_{ge}(n)/n\right]/\mu_{ge}(1)$, where $\mu_{ge}(n)$ is the modulus of the transition dipole moment of the H-aggregate formed by n DO3 molecules, and $\mu_{ge}(1)$ is the transition dipole moment of the monomer. By taking $\mu_{ge}(n)/n$ we consider the average contribution to the transition dipole of the aggregate originating from one molecule within

the aggregate. Hence, the $[\mu_{ge}(n)/n]/\mu_{ge}(1)$ ratio indicates how intermolecular interaction within the aggregate may influence, on the average, the molecular contribution to the electronic transition of the aggregate. Of course, for negligible intermolecular interactions, the ratio is close to 1. Moreover, since the experimental value $\mu_{ge}(C)$ is determined from $\varepsilon(C)$, by considering the nominal molar concentration of the solution (i.e., moles of DO3 per unit volume), it turns out that the quantity $\mu_{ge}(C)$ represents the average value of the transition dipole of DO3, independently of its aggregation state. Therefore, $\mu_{ge}(C)/\mu(dil)$ is the experimental proxy of the quantity $[\mu_{ge}(n)/n]/\mu_{ge}(1)$ that we have determined by TDDFT calculations.

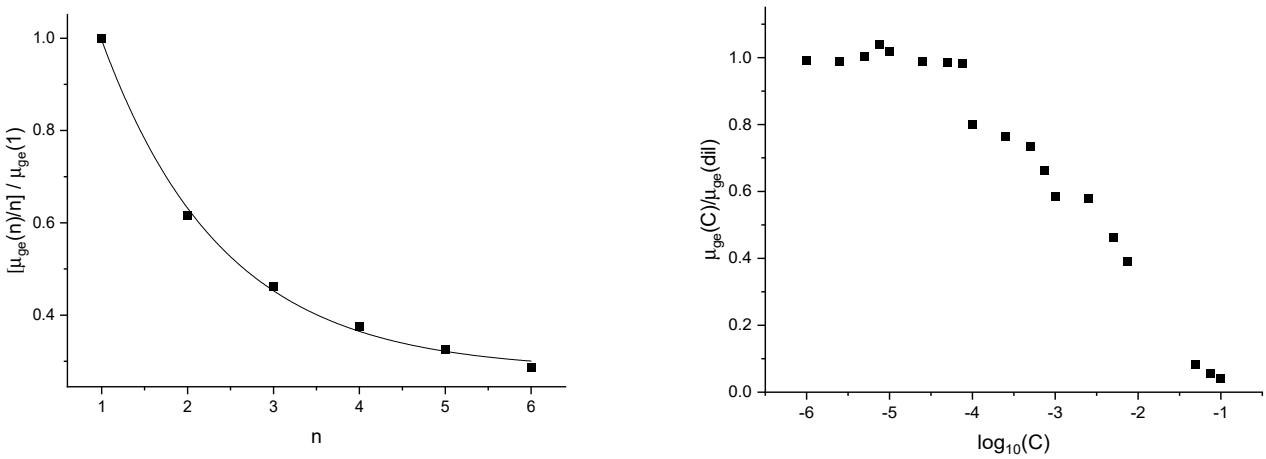

(**a**) (**b**)

Figure 4. (**a**) Plot of the ratios $[\mu_{ge}(n)/n]/\mu_{ge}(1)$ vs. the number of monomeric units (n) forming the aggregates, as determined by TDDFT calculations. The fit is reported to guide the eye and extrapolates to 0.28 for $n \to \infty$. (**b**) Plot of the ratios $\mu_{ge}(C)/\mu_{ge}(dil)$ with respect to the logarithm of the molar concentration of DO3 in DMSO. The $\mu_{ge}(dil)$ value was obtained from the square root of the average value of the ε determined from the diluted solutions (C < 10^{-4} M).

The decreasing trends shown in Figure 4 indicate that the transition dipole moment is significantly influenced by the formation of H-aggregates. Notably, TDDFT calculations indicate that the transition dipole moment of the hexamer is less than one-third of the transition dipole moment of the monomer. Similarly, when comparing the experimental counterpart (Figure 4b), we observe a similar decrease: the transition dipole moment at the 10^{-2}M concentration is around one-third of the transition dipole moment of the diluted solutions. At higher concentrations, the observed transition dipole moment decreases further, to values that are even lower than those that can be extrapolated from Figure 4a for large n values. We think this indicates the formation of other kinds of aggregates that have not been considered in our present DFT analysis. This is reasonable, since at increasingly large concentrations the formation of seeds of three-dimensional nanocrystals is expected, and these could be formed by, e.g., side-by-side stacks of H-aggregates, where the interactions among the DO3 molecules are different from those in H-aggregates. Therefore, it is not surprising that the transition dipole moment displays different trends in different concentration ranges.

As discussed above (see Figure 2), Raman spectroscopy as well is sensitive to aggregation phenomena, even though it is not applicable through such a wide concentration range as UV-Vis spectroscopy. This is due to intrinsic reasons, due to the inherent weakness of the Raman scattering process compared with photon absorption. It is thus interesting to correlate the behavior of the Raman cross-section ratio (σ_a/σ_s) with the molar extinction coefficient ε, as reported in Figure 5, which shows a clear monotonic trend where a high ratio of Raman cross-sections (at low concentrations) corresponds to high molar extinction coefficients. This evident experimental observation can be justified by a straightforward

theoretical analysis of the Raman cross-section. Since we work in near-resonance conditions, we consider the doubly resonant term in the Nafie–Peticolas–Stein expression of the Raman polarizability (α), which leads to [27,28]:

$$\sigma \propto \alpha^2 \propto \left[\frac{\mu_{ge}^2 \langle e | \frac{\partial H}{\partial q} | e \rangle}{\left(\hbar\omega_{ge} - \hbar\omega_l\right)^2} \right]^2 \tag{2}$$

We recognize the presence of the same transition dipole moment which directly determines the molar absorptivity ε. Hence the expression for the Raman cross-section can be simplified as follows:

$$\sigma \propto \varepsilon^2 \frac{g^2}{\Delta E^4} \tag{3}$$

where $g = \langle e | \frac{\partial H}{\partial q} | e \rangle$ is the vibronic coupling matrix element and $\Delta E = \hbar\omega_{ge} - \hbar\omega_l$ is the difference between the transition energy to the excited state and the photon energy of the laser used in the Raman experiment. Equation (3) clearly justifies the monotonic relationship observed between σ and ε. Interestingly, since the data in Figure 5 display a quadratic behavior only above a concentration of about 10^{-3} M, we conclude that the $g^2/\Delta E^4$ term is weakly dependent on concentration only for high concentrations.

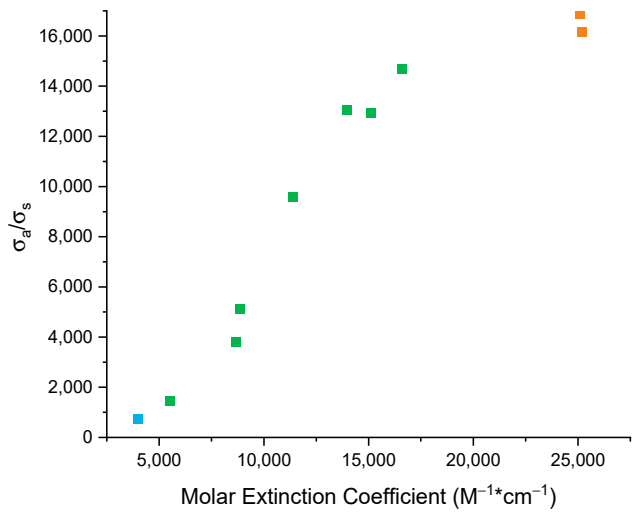

Figure 5. Plot of the ratio of the Raman cross-section (σ_a/σ_s) vs. the molar extinction coefficient (ε) of DO3 in DMSO at varying concentrations (red < 10^{-4} M, green between 10^{-4} M and 10^{-2} M, and blue > 10^{-2} M).

5. Conclusions

By combining UV-Vis absorption, Raman spectroscopy, and DFT calculations, we could characterize the formation of molecular H-aggregates of Disperse Orange 3 (DO3) in a wide range of concentrations in DMSO. The aggregation in DMSO starts at roughly 10^{-4} M, as inferred from the relationship between the molar absorptivity and the transition dipole moment. The findings show the presence of H-aggregates made up of variable numbers of DO3 molecules as the concentration rises. As the concentration increases, the data indicate the coexistence of H-aggregates comprised of a varying number of DO3 molecules. Moreover, based on the peak position in the UV-Vis absorption spectrum and the observed relative decrease in the transition dipole moment, we estimate the substantial presence of H-aggregates formed by four DO3 molecules at a concentration of about 10^{-2}M. In more concentrated solutions (10^{-1} M), the trend of the transition dipole moment shifts, indicating the emergence of higher aggregates that may be compared to the seeds of nanocrystals. The data from Raman spectroscopy support the formation of H-aggregates based on the shift in the N=N stretching mode with increasing concentration. Additionally,

the established theory of resonance Raman justifies the monotonic correlation between the molar absorption coefficient and the dependency on the concentration of the Raman cross-section ratio through the transition dipole moment.

For future studies, our interest has now shifted to the phenomena that occur at higher concentrations. Our hypothesis is that above a certain concentration, nanoaggregates turn into nano-crystal seeds. For instance, TDDFT calculations on a model composed of two H-aggregate trimers of DO3 interacting side-by-side provide a lower value of the $[\mu_{ge}(n)/n]/\mu_{ge}(1)$ ratio than the fully stacked H-aggregate hexamer (i.e., 0.23 vs. 0.29), which confirms the role of more complex aggregates in the experimental data at high concentrations. The combination of DFT simulations and dynamic light scattering techniques could allow us to collect new data to apply the method presented here at higher concentrations ranges.

Author Contributions: V.S. analyzed the experimental data. V.S., M.D. and P.M. performed the UV-Vis spectroscopy experiments. V.S. and A.L. performed the Raman spectroscopy experiments. M.T. performed the TDDFT simulations. V.S., P.M. and R.C. wrote the paper taking into consideration the input of all authors. C.B. and M.T. conceived the work, planned experiments, and provided resources. The manuscript was written through contributions of all authors. All authors have read and agreed to the published version of the manuscript.

Funding: C.B. acknowledges the PRIN 2020 project (ID 2020XBFEMS) from The Italian Ministry for Universities and Research.

Data Availability Statement: The data presented in this study are available on request from the corresponding author.

Acknowledgments: M.T. acknowledges support from the European Union—Next Generation EU through the Italian National Centre for HPC, Big Data and Quantum Computing.

Conflicts of Interest: The authors declare no conflict of interest.

References

1. Zheng, Y.-Q.; Yao, Z.-F.; Dou, J.-H.; Wang, Y.; Ma, W.; Zou, L.; Nikzad, S.; Li, Q.-Y.; Sun, Z.-H.; Yu, Z.-A.; et al. Influence of Solution-State Aggregation on Conjugated Polymer Crystallization in Thin Films and Microwire Crystals. *Giant* **2021**, *7*, 100064. [CrossRef]
2. Penn, R.L. Kinetics of Oriented Aggregation. *J. Phys. Chem. B* **2004**, *108*, 12707–12712. [CrossRef]
3. De Yoreo, J.J.; Nakouzi, E.; Jin, B.; Chun, J.; Mundy, C.J. Spiers Memorial Lecture: Assembly-Based Pathways of Crystallization. *Faraday Discuss.* **2022**, *235*, 9–35. [CrossRef] [PubMed]
4. Zhang, L.; Cole, J.M. Dye Aggregation in Dye-Sensitized Solar Cells. *J. Mater. Chem. A* **2017**, *5*, 19541–19559. [CrossRef]
5. LaPlante, S.R.; Carson, R.; Gillard, J.; Aubry, N.; Coulombe, R.; Bordeleau, S.; Bonneau, P.; Little, M.; O'Meara, J.; Beaulieu, P.L. Compound Aggregation in Drug Discovery: Implementing a Practical NMR Assay for Medicinal Chemists. *J. Med. Chem.* **2013**, *56*, 5142–5150. [CrossRef]
6. LaPlante, S.R.; Roux, V.; Shahout, F.; LaPlante, G.; Woo, S.; Denk, M.M.; Larda, S.T.; Ayotte, Y. Probing the Free-State Solution Behavior of Drugs and Their Tendencies to Self-Aggregate into Nano-Entities. *Nat. Protoc.* **2021**, *16*, 5250–5273. [CrossRef] [PubMed]
7. Doudevski, I.; Schwartz, D.K. Concentration Dependence of Self-Assembled Monolayer Island Nucleation and Growth. *J. Am. Chem. Soc.* **2001**, *123*, 6867–6872. [CrossRef]
8. Hestand, N.J.; Spano, F.C. Expanded Theory of H- and J-Molecular Aggregates: The Effects of Vibronic Coupling and Intermolecular Charge Transfer. *Chem. Rev.* **2018**, *118*, 7069–7163. [CrossRef] [PubMed]
9. Ma, S.; Du, S.; Pan, G.; Dai, S.; Xu, B.; Tian, W. Organic Molecular Aggregates: From Aggregation Structure to Emission Property. *Aggregate* **2021**, *2*, e96. [CrossRef]
10. Ouyang, C.; Chen, S.; Che, B.; Xue, G. Aggregation of Azo Dye Orange I Induced by Polyethylene Glycol in Aqueous Solution. *Colloids Surf. A Physicochem. Eng. Asp.* **2007**, *301*, 346–351. [CrossRef]
11. Hamada, K.; Miyawaki, E.; Jaung, J. The Effect of Substituents on the Aggregation and Gelation of Azo Sulphonate Dyes. *Color. Technol.* **2005**, *121*, 127–131. [CrossRef]
12. Kuiper, J.M.; Engberts, J.B.F.N. H-Aggregation of Azobenzene-Substituted Amphiphiles in Vesicular Membranes. *Langmuir* **2004**, *20*, 1152–1160. [CrossRef] [PubMed]
13. Skrabal, P.; Bangerter, F.; Hamada, K.; Iijima, T. Entropy Contribution to an Azo Dye Aggregation in Aqueous Solution. *Dye. Pigment.* **1987**, *8*, 371–374. [CrossRef]

14. Karukstis, K.K.; Perelman, L.A.; Wong, W.K. Spectroscopic Characterization of Azo Dye Aggregation on Dendrimer Surfaces. *Langmuir* **2002**, *18*, 10363–10371. [CrossRef]
15. Cuétara-Guadarrama, F.; Vonlanthen, M.; Sorroza-Martínez, K.; González-Méndez, I.; Rivera, E. Photoisomerizable Azobenzene Dyes Incorporated into Polymers and Dendrimers. Influence of the Molecular Aggregation on the Nonlinear Optical Properties. *Dye. Pigment.* **2021**, *194*, 109551. [CrossRef]
16. Milani, A.; Brambilla, L.; Del Zoppo, M.; Zerbi, G. Raman Dispersion and Intermolecular Interactions in Unsubstituted Thiophene Oligomers. *J. Phys. Chem. B* **2007**, *111*, 1271–1276. [CrossRef]
17. Flynn, J.D.; Lee, J.C. Raman Fingerprints of Amyloid Structures. *Chem. Commun.* **2018**, *54*, 6983–6986. [CrossRef]
18. Cazzolli, G.; Caponi, S.; Defant, A.; Gambi, C.M.C.; Marchetti, S.; Mattarelli, M.; Montagna, M.; Rossi, B.; Rossi, F.; Viliani, G. Aggregation Processes in Micellar Solutions: A Raman Study. *J. Raman Spectrosc.* **2012**, *43*, 1877–1883. [CrossRef]
19. Bandara, H.M.D.; Burdette, S.C. Photoisomerization in Different Classes of Azobenzene. *Chem. Soc. Rev.* **2012**, *41*, 1809–1825. [CrossRef]
20. Piyanzina, I.; Minisini, B.; Tayurskii, D.; Bardeau, J.-F. Density Functional Theory Calculations on Azobenzene Derivatives: A Comparative Study of Functional Group Effect. *J. Mol. Model.* **2015**, *21*, 34. [CrossRef] [PubMed]
21. Pilot, R.; Signorini, R.; Durante, C.; Orian, L.; Bhamidipati, M.; Fabris, L. A Review on Surface-Enhanced Raman Scattering. *Biosensors* **2019**, *9*, 57. [CrossRef] [PubMed]
22. Frisch, M.J.; Trucks, G.W.; Schlegel, H.B.; Scuseria, G.E.; Robb, M.A.; Cheeseman, J.R.; Scalmani, G.; Barone, V.; Mennucci, B.; Petersson, G.A.; et al. *Gaussian 09, Revision D.01*; Gaussian, Inc.: Wallingford, CT, USA, 2009.
23. Freyer, W.; Brete, D.; Schmidt, R.; Gahl, C.; Carley, R.; Weinelt, M. Switching Behavior and Optical Absorbance of Azoben-zene-Functionalized Alkanethiols in Different Environments. *J. Photochem. Photobiol. A Chem.* **2009**, *204*, 102–109. [CrossRef]
24. Deslippe, J.; Samsonidze, G.; Strubbe, D.A.; Jain, M.; Cohen, M.L.; Louie, S.G. BerkeleyGW: A Massively Parallel Computer Package for the Calculation of the Quasiparticle and Optical Properties of Materials and Nanostructures. *Comput. Phys. Commun.* **2012**, *183*, 1269–1289. [CrossRef]
25. Schellman, J.A. Circular Dichroism and Optical Rotation. *Chem. Rev.* **1975**, *75*, 323–331. [CrossRef]
26. Zanchi, C.; Longhi, G.; Abbate, S.; Pellegrini, G.; Biagioni, P.; Tommasini, M. Evaluation of Molecular Polarizability and of Intensity Carrying Modes Contributions in Circular Dichroism Spectroscopies. *Appl. Sci.* **2019**, *9*, 4691. [CrossRef]
27. Peticolas, W.L.; Nafie, L.; Stein, P.; Fanconi, B. Quantum Theory of the Intensities of Molecular Vibrational Spectra. *J. Chem. Phys.* **1970**, *52*, 1576–1584. [CrossRef]
28. Tommasini, M.; Castiglioni, C.; Zerbi, G. Raman Scattering of Molecular Graphenes. *Phys. Chem. Chem. Phys.* **2009**, *11*, 10185. [CrossRef]

Disclaimer/Publisher's Note: The statements, opinions and data contained in all publications are solely those of the individual author(s) and contributor(s) and not of MDPI and/or the editor(s). MDPI and/or the editor(s) disclaim responsibility for any injury to people or property resulting from any ideas, methods, instructions or products referred to in the content.